Aβ-induced NOX2 activation underlies oxidative stress leading to brain hypometabolism and hyperactivity in Alzheimer's disease

Anton Malkov[1†], Irina Popova[1†], Anton Ivanov[2], Sung-Soo Jang[3], Seo Yeon Yoon[3], Alexander Osypov[1,4], Yadong Huang[3,5], Yuri Zilberter[2†], Misha Zilberter[3†*]

[1]*Institute of Theoretical and Experimental Biophysics, Russian Academy of Sciences, 142290, Pushchino, Russia.*
[2]*Aix Marseille Université, Inserm, INS UMR_S 1106, 13005, Marseille, France.*
[3]*Gladstone Institute of Neurological Disease, San Francisco, CA 94158, USA.*
[4]*Institute of Higher Nervous Activity and Neurophysiology, Russian Academy of Sciences, 117485, Moscow, Russia.*
[5]*Department of Neurology, University of California, San Francisco, CA 94158, USA.*

Single sentence summary:

NADPH oxidase inhibition prevents beta amyloid-induced brain hypometabolism and network hyperactivity, suggesting a novel therapeutic approach for Alzheimer's disease.

[†]Authors contributed equally

* To whom correspondence should be addressed:

misha.zilberter@gladstone.ucsf.edu

Abstract

A paramount driver of sporadic Alzheimer's disease (AD) is the synergy of oxidative stress and glucose hypometabolism in the brain. Oxidative stress damages cellular macromolecules such as DNA, lipids and proteins, whereas glucose hypometabolism impairs cellular energy supply and antioxidant defence; Together, these cellular and functional alterations may be primary triggers of AD. However, the exact molecular basis of AD-associated glucose hypometabolism has remained unknown, hampering the search for effective interventions. Here, we identify NADPH oxidase 2 (NOX2) activation by beta-amyloid peptide ($A\beta_{1-42}$) as the main molecular source of oxidative stress driving brain glucose hypometabolism and network hyperactivity. Using a combination of electrophysiology with dynamic recordings of autofluorescence and metabolic biosensors, we show that in hippocampal brain slices, $A\beta_{1-42}$ application reduced network activity-driven glucose consumption and glycolysis by half, while NOX2 antagonism prevented this effect. *In vivo*, intracerebroventricular injection of $A\beta_{1-42}$ exerted a profound inhibitory effect on brain glucose consumption, resulting in long-lasting network hyperactivity and changes in animal behavioral profile. Critically, the novel bioavailable NOX2 antagonist GSK2795039 prevented all of the observed Aβ-related detrimental effects. These data suggest that targeting NOX2-induced oxidative stress is a promising approach to both the prevention and treatment of AD.

Introduction

The pathological processes that drive AD may begin several decades before the first clinical symptoms manifest *(1–3)*. Numerous human studies suggest a causal upstream role for Aβ in AD pathogenesis *(3–5)*. Although β-amyloidosis alone may not be sufficient to cause cognitive deterioration, it likely causes downstream pathological changes (i.e., tauopathy and neurodegeneration) that ultimately lead to cognitive decline *(3, 6)*. Recent progress in AD biomarkers has revealed that amyloidosis is one of the earliest signs of AD pathogenesis, detectable at preclinical stages of the disease *(1–3)*. Interestingly, at this stage patients are still cognitively unimpaired but may demonstrate variable neuropsychiatric symptoms (e.g., apathy, depression, agitation/aggression, anxiety, and irritability) *(7, 8)*, the emergence of which may correlate with amyloidosis *(9)*.

Initial Aβ pathology is often detected concurrently with another pre-symptomatic marker of AD, glucose hypometabolism *(10–12) (13)*. Indeed, glucose hypometabolism is an accurate predictor of progression to AD in mild cognitive impairment (MCI) patients *(10, 14, 15)*. Since glucose utilization underlies vital brain functions such as energy supply and antioxidant defence *(16)*, it is not surprising that disturbances in glucose metabolism can lead to a chain of harmful consequences, and thus likely represent a major underlying cause of disease initiation and progression *(12)*. In turn, multiple studies have shown that oligomeric Aβ induces oxidative stress *(12, 17),* which has been hypothesized to inhibit glucose metabolism during AD *(12, 18)*, thus establishing a vicious cycle of disease initiation and progression. Thus, early brain glucose hypometabolism may prove to be the crucial link between Aβ accumulation *(19, 20)* and subsequent neurodegeneration in the chain of AD progression. However, until now the exact trigger for AD-associated glucose hypometabolism has been unknown, hampering the search for effective treatment.

In the current study, we found that oxidative stress specifically caused by the $A\beta_{1-42}$ -induced activation of NAD(P)H oxidase (NOX) underlies glucose metabolism deficiency. It was previously reported in multiple cell types that $A\beta_{1-42}$ induces brain oxidative stress *(21),* largely via activation of NOX *(22–24)*. We show *in vivo* that NOX activation by oligomeric $A\beta_{1-42}$ results in pathological changes in brain glucose consumption, hippocampal network hyperactivity, and neuropsychiatric-like disturbances in the behavior of mice—all abnormalities that can be prevented by administration of the novel selective NOX2 antagonist GSK2795039. Therefore, NOX may be a primary molecular target responsible for AD initiation and progression. Our results suggest that early intervention in NOX-induced oxidative stress has the potential to be an effective approach to AD prevention and treatment.

Results

$A\beta_{1-42}$ disrupts network glucose utilization both in brain slices and in vivo

Our previous publication suggested that $A\beta_{1-42}$ modifies glycolysis when applied to brain slices *(25)*. To investigate this effect further, we applied fibrillar $A\beta_{1-42}$ to hippocampal slices for 40 minutes, which acutely and robustly reduced network activity-driven glucose uptake in hippocampal slices to 57.7 ± 4.13% of control ($p < 0.0001$, $n = 21$) (Fig. 1A). To confirm this result *in vivo*, we injected $A\beta_{1-42}$ i.c.v. in anesthetized mice. In the living brain, the dynamics of extracellular glucose differ from brain slices where there is a constant supply of glucose from the perfusate (in our case, 5mM), and any glucose uptake is seen as a negative deflection in extracellular glucose levels (Fig. 1A). *In vivo*, network activation also leads to an increase in glucose uptake, but the blood vessels rapidly dilate and the supply of glucose is upregulated,

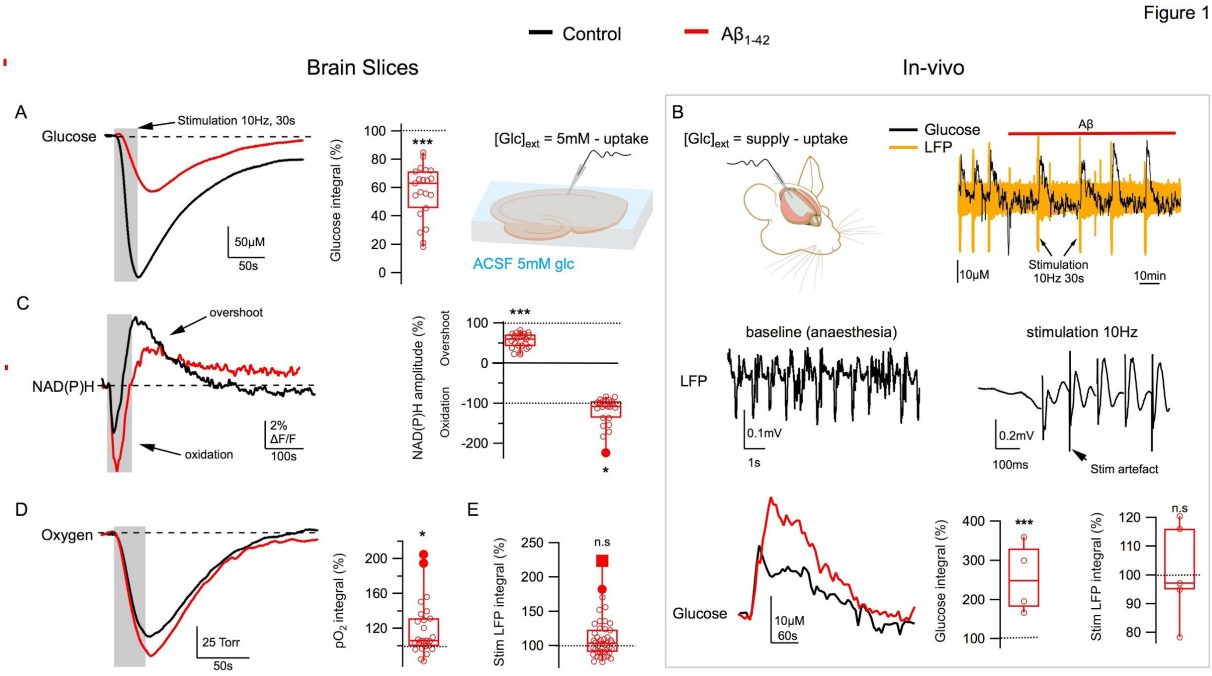

Figure 1. ***Aβ$_{1-42}$ acutely inhibits network glucose utilization.*** **A.** In brain slices, fibrillar Aβ$_{1-42}$ reduces network activity-driven glucose uptake. *Left*, example traces from a single experiment showing the extracellular glucose transients in CA1 pyramidal cell layer in response to a 10Hz, 30s stimulation of Schaffer collaterals (grey) in control (black) and following 40min of Aβ$_{1-42}$ application (red). Considering the constant 5mM glucose supply from the perfusate, the drop in the transient amplitude indicates reduced uptake. *Middle*, summary graph showing glucose transient integral values normalized to controls. **B.** In anesthetized mice, i.c.v. injection of fibrillar Aβ$_{1-42}$ results in a rapid change in glucose uptake. *Top left*, a schematic depicting the relationship between the dynamic extracellular glucose supply from the blood (which increases following synaptic activation) and network glucose uptake. *Top right:* example traces from a single experiment showing both local field potential (LFP, orange) and extracellular glucose (black) recordings from the CA1 region before and after Aβ$_{1-42}$ injection. *Middle row:* in detail of LFP recording showing characteristic anaesthesia-induced oscillations (left) at baseline and the response to synaptic stimulation (right). *Bottom row,* average stimulation-induced glucose transients from a single experiment in control (black) and following i.c.v. Aβ$_{1-42}$ injection (red). *Middle*, summary graph showing glucose transient integral values normalized to controls; *right*, a summary of LFP integrals showing that stimulation response did not change significantly following Aβ$_{1-42}$ injection; This suggests that the activity-induced increase in glucose supply from the blood did not change, and therefore the apparent increase in glucose transients following Aβ$_{1-42}$ injection indicates reduced uptake. **C.** Aβ$_{1-42}$ inhibits activity-driven glycolysis. *Left*, NAD(P)H autofluorescence traces from a single experiment in control (black) and following 40min of Aβ$_{1-42}$ application (red). *Right,* summary values of transient amplitudes both for the "overshoot" (glycolysis-related) and "oxidation" phases of the signal. **D.** Aβ$_{1-42}$ increases oxygen consumption: sample pO_2 traces from a single experiment showing a transient decrease of tissue oxygen levels in control (black) and following 40min of Aβ$_{1-42}$ application (red) and a summary plot of normalized pO_2 integral values. **E.** Aβ$_{1-42}$ does not significantly change the strength of network response to synaptic stimulation: a summary plot of normalized LFP train integral values. *p <0.05, ***p<0.01.

leading to a net increase of extracellular glucose, as has been demonstrated in response to sensory stimulation *(26)* or electric stimulation *(27)*. Following Aβ$_{1-42}$ injection, extracellular glucose transients increased in response to synaptic stimulation more than two-fold (248.5 ± 45% of control; $p < 0.0005$; $n = 5$) (Fig. 1B). Meanwhile, network LFP response to stimulation

did not change significantly (Fig. 1B, bottom right), nor did the baseline glucose concentration (not shown), suggesting that Aβ did not affect glucose delivery and that the increased amplitudes of the extracellular glucose transients likely indicate a reduced uptake of glucose by the activated network, mirroring the results obtained in brain slices.

We also observed that $A\beta_{1-42}$ decreased glycolysis, seen as reduced amplitudes of NAD(P)H fluorescence "overshoot" (56.4 ± 3.8% of control; $p < 0.0001$; n = 23) (Fig. 1C), together with an increase of oxidation ("dip") amplitude (118.6 ± 7.55% of control; $p < 0.03$; n = 23) *(28)*. In line with this, we observed a significant increase in activity-driven oxygen consumption (118.7 ± 6%; $p < 0.005$; n = 26) (Fig. 1D), which together with increased NAD(P)H oxidation amplitude could indicate upregulated mitochondrial respiration to compensate for reduced glycolysis *(29, 30)*. Finally, none of these disruptions could be attributed to changes in stimulation strength or response, as the stimulus train LFP integral did not change (102.6 ± 3.96% of control, n=21) (Fig. 1E).

$A\beta_{1-42}$ toxicity is prevented by blockade of NOX2

The changes in glucose utilization resulting from $A\beta_{1-42}$ treatment were similar to those we previously observed following induced seizures, which are paralleled by a spike of H_2O_2 release *(31)*. In that context, the likely source of the H_2O_2 and actual trigger of seizures is the reactive oxygen species (ROS)-generating NAD(P)H oxidase (NOX) *(32)*. $A\beta_{1-42}$ has been reported to induce oxidative stress in multiple cell types by activating NOX *(21–24)*. Therefore, we asked whether the toxic effect of Aβ on glucose metabolism was mediated by NOX activation. Indeed, when NOX2 was inhibited by the novel NOX2 antagonist GSK2795039, $A\beta_{1-42}$ failed to disrupt glucose uptake in slices (Fig. 2A) or *in vivo* (Fig. 2B). NOX2 inhibition also prevented $A\beta_{1-42}$-induced modification of glycolysis (Fig. 2C) or oxygen consumption (Fig. 2D).

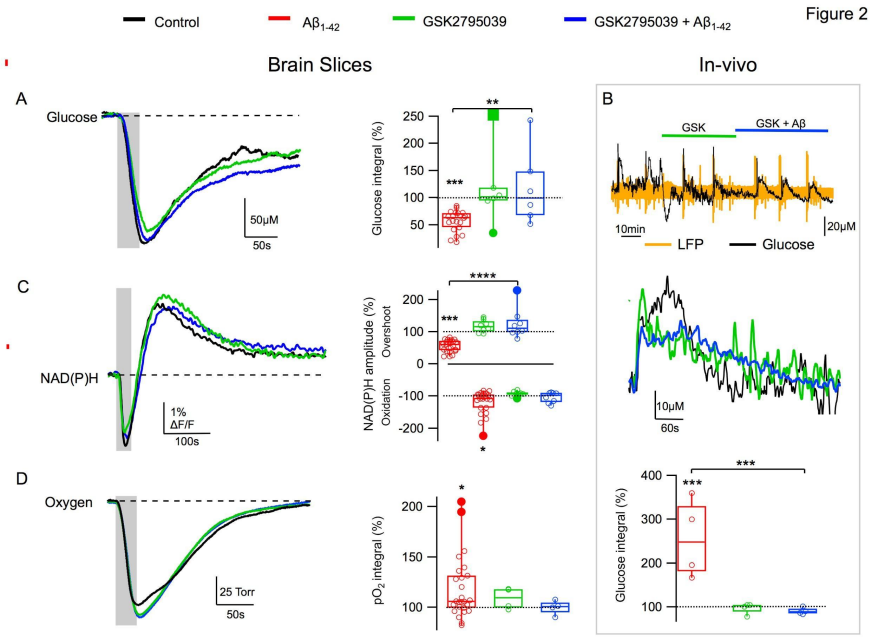

Figure 2. ***NOX2 blockade prevents Aβ$_{1-42}$ –induced disruption of network glucose utilization.***
A. In brain slices, application of NOX2 antagonist GSK2795039 prevents the reduction in network activity-driven glucose uptake caused by Aβ$_{1-42}$: example traces from a single experiment showing the extracellular glucose transients in CA1 pyramidal cell layer in response to a 10Hz, 30s stimulation of Schaffer collaterals (grey) in control (black), after wash-in of GSK2795039 (green), and following 40min of GSK2795039 + Aβ$_{1-42}$ application (blue); summary graph showing corresponding glucose transient integral values normalized to controls with those of Aβ$_{1-42}$ alone for comparison (red). **B.** In anesthetized mice, intraventricular injection of GSK2795039 + Aβ$_{1-42}$ (blue) preceded by GSK2795039 (green) fails to elicit any changes in glucose uptake. *Top*, example traces from a single experiment showing both local field potential (LFP, orange) and extracellular glucose (black) recordings from the CA1 region. *Middle*, average stimulation-induced glucose transients from a single experiment in control (black), following i.c.v. GSK2795039 injection (green) and subsequent injection of GSK2795039 + Aβ$_{1-42}$ (blue). *Bottom*, the summary graph showing corresponding glucose transient integral values together with those of Aβ$_{1-42}$ alone for comparison (red). **C.** GSK2795039 prevents Aβ$_{1-42}$ disruption of activity-driven glycolysis. *Left*, NAD(P)H autofluorescence traces from a single experiment in control (black) after wash-in of GSK2795039 (green), and following 40min of GSK2795039 + Aβ$_{1-42}$ application (blue); *Right,* summary values of transient amplitudes both for the "overshoot" (glycolysis-related) and "oxidation" phases of the signal. **D.** GSK2795039 blocks Aβ$_{1-42}$ induced increase in oxygen consumption: sample pO_2 traces from a single experiment showing a transient decrease of tissue oxygen levels in control (black) after wash-in of GSK2795039 (green), and following 40min of GSK2795039 + Aβ$_{1-42}$ application (blue); the summary plot of normalized pO_2 integral values. *p <0.05, ***p<0.01, ****p<0.001.

Aβ$_{1-42}$ disruption of glucose utilization is replicated by NOX activator PMA

We then tested whether pharmacological activation of NOX2 mimics the effect of Aβ$_{1-42}$ on glucose utilization using the NOX activator phorbol 12-myristate 13-acetate (PMA, 100 nM) *(33)*. Strikingly, application of PMA to brain slices reproduced the effect of Aβ$_{1-42}$, resulting in a reduction of both the glucose consumption to 68.5 ± 6.4% of control ($p<0.0001$; n = 10) (Fig. 3A,C), and NAD(P)H overshoot (glycolysis) to 70.7 ± 4.8% of control ($p<0.0001$; n = 12) (Fig. 3B,C). Curiously, PMA treatment did not significantly alter either the NAD(P)H oxidative phase amplitude (Fig. 3D,F) or oxygen consumption (data not shown), suggesting a lack of effect on respiration. Accordingly, NOX2 antagonist GSK2795039 completely prevented the PMA effects (Fig. 3B-F). Importantly, it has been reported that GSK2795039 has no indirect action on PMA

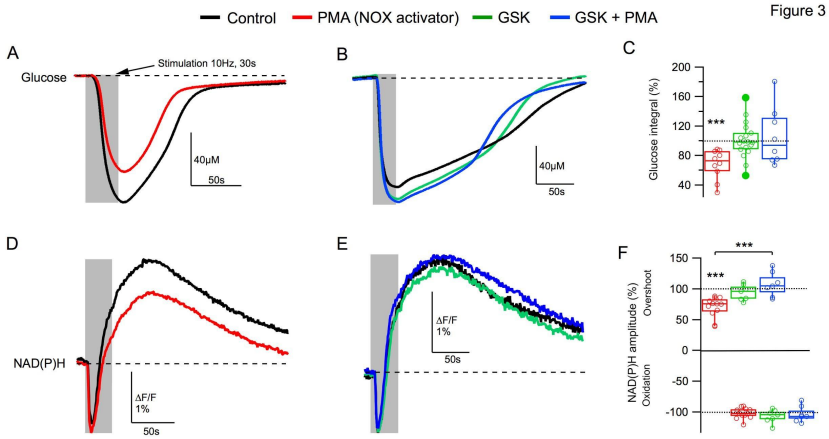

Figure 3. ***Direct activation of NOX reproduces the effect of*** **Aβ$_{1-42}$** ***on glucose utilization***. **A.** Application of NOX activator PMA (100nM) reduces glucose uptake; average traces from a single experiment showing extracellular glucose transients in CA1 pyramidal cell layer in response to a 10Hz, 30s stimulation of Schaffer collaterals (grey) in control (black) and following 40min of PMA application (red) **B.** GSK2795039 prevents the effects of PMA on activity-driven glycolysis. Example traces from a single experiment showing glucose transients in control (black), after application of GSK2795039 (green), and following GSK2795039+PMA application (blue). **C**. Summary graph of all corresponding glucose transient integral values in A-B. **D**. PMA reduces glycolysis: NAD(P)H autofluorescence traces from a single experiment in control (black) and after application of PMA (red). **E**. PMA effect on glycolysis is blocked by GSK2795039: NAD(P)H autofluorescence traces from a single experiment in control (black), after application of GSK2795039 (green), and following GSK2795039+PMA application (blue). **F**. Summary graph of all corresponding NAD(P)H amplitudes in D-E. ***p<0.01

and therefore its effect is likely mediated by NOX2 inhibition alone *(34)*. Taken together, these data suggest that Aβ$_{1-42}$ inhibits glucose metabolism by inducing oxidative stress via NOX2 activation.

Neuronal NOX2 expression is largely responsible for the effects of Aβ$_{1-42}$

In the brain, NOX2 is primarily expressed in microglia *(35, 36)*, although it is also present in neurons *(37)* and astrocytes *(38)*. To begin to determine in which cell type Aβ$_{1-42}$ affects NOX2, we recorded activity-driven NAD(P)H transients before and after Aβ$_{1-42}$ application in the presence of the NMDA receptor blocker APV. NMDA receptors are primarily expressed in neurons and neuronal NOX2 is activated via the NMDA receptor signaling pathway *(39)*. Moreover, inhibiting NMDA receptors abolishes NOX2-induced epileptic seizures *(32)*. The addition of APV by itself had no effect on NAD(P)H transients, but it prevented Aβ-induced modifications (Fig. 4A). This indicates that activation of NOX2 by Aβ is largely dependent on NMDA receptor signaling. Next, to determine any potential microglial involvement in the effect of Aβ$_{1-42}$, we artificially reduced microglial density by feeding mice chow containing PLX5622, an inhibitor of colony-stimulating factor 1 receptor (CSF1R) which results in microglia depletion *(40, 41)*.

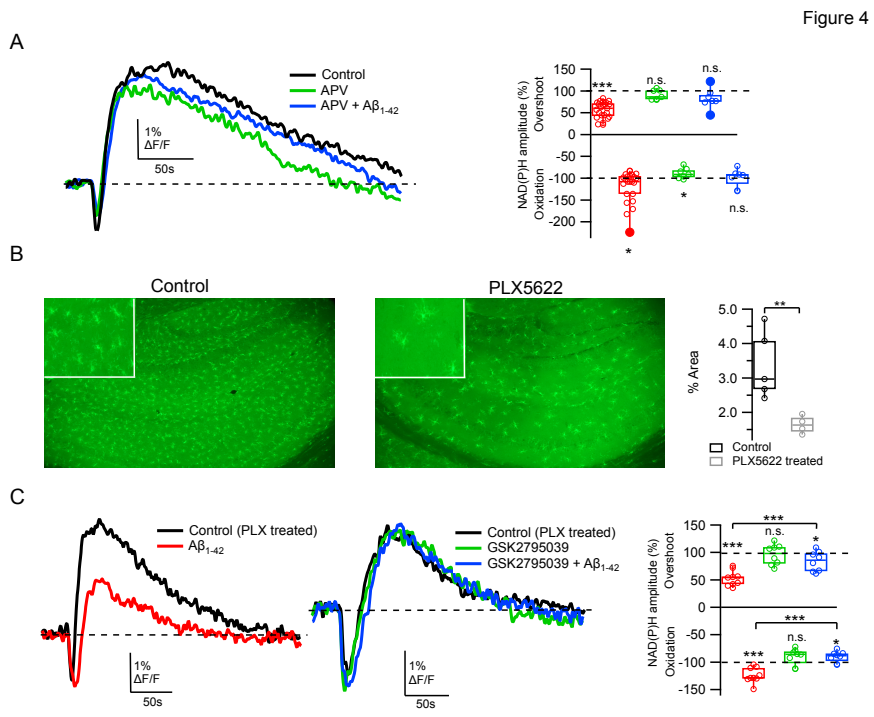

Figure 4. ***Locus of NOX2 expression behind Aβ-induced glucose hypometabolism.*** **A.** NMDA receptor blockade by APV prevents Aβ effects on glycolysis, suggesting neuronal NOX contribution. Left, example traces from a single experiment showing activity-induced NAD(P)H autofluorescence transients in control (black), following APV application (green), and after subsequent application of $A\beta_{1-42}$ (blue). Right, the summary plot of NAD(P)H oxidation and overshoot amplitudes; red markers indicate Aβ values from Fig. 1 for comparison. **B, C.** Microglial depletion does not prevent Aβ effect on glucose utilization. **B.** Sample images of *ex-vivo* hippocampal microsections stained for lba1 antibody from mice following 1 week of control (left) and PLX5622-containing diet (center). Right, quantification of GFP fluorescence % area. **C.** Hippocampal slices from PLX5622-treated mice are not protected from Aβ toxicity on glucose utilization. Left, traces from a single experiment showing activity-induced NAD(P)H autofluorescence transients in control (black) and following application of $A\beta_{1-42}$ (red). Center: NOX2 blockade in microglia-depleted slices prevents Aβ effects on glycolysis. Right: summary plot of corresponding NAD(P)H amplitudes. *p<0.05, **p<0.02, ***p<0.01.

One week of PLX5622 diet reduced hippocampal microglia density to 48.8% of controls (area 1.64 ± 0.13% vs. 3.37 ± 0.44% in controls, p = 0.02) (Fig. 4B). Nevertheless, in microglia-depleted slices, addition of $A\beta_{1-42}$ significantly reduced the activity-driven NAD(P)H overshoot amplitude to 58 ± 4.97% of control (n = 9, p < 0.0001) (Fig. 4C) and increased dip amplitude to 114 ± 4.92% of control (n = 9, p = 0.003) (Fig. 4C), similar to the effect in slices from non-depleted mice (overshoot reduction: p = 0.54; oxidation increase: p = 0.18). Moreover, NOX2 antagonist GSK2795039 again prevented the $A\beta_{1-42}$ effect (Fig. 4C), indicating a significant presence of functional NOX2 in the microglia-depleted slices. Altogether, these results suggest that the effect of $A\beta_{1-42}$ is mediated by NOX2 in neurons, although we cannot completely rule out microglial involvement due to potential NMDAR expression in microglia as well as incomplete microglial depletion in this study.

NOX2 inhibition prevents $A\beta_{1-42}$-induced hyperexcitability in vivo

Epileptic seizures are a frequent comorbidity of AD *(42, 43)*. Epilepsy also occurs in multiple transgenic models overproducing Aβ *(44)*, and network hyperactivity has been observed in hippocampal slices following acute Aβ application *(25, 45)*. To investigate the immediate and medium-term effects of $A\beta_{1-42}$ on network electrophysiology, we recorded hippocampal CA1 local field potentials in awake freely-moving wild type mice before and following i.c.v. oligomeric $A\beta_{1-42}$ injection. We observed a rapid onset of network hyperactivity following $A\beta_{1-42}$ injection, seen both as an increased accumulative activity (a general measure of high network activity) *(46)* and in interictal spike frequency (Fig. 5A, C). Network hyperactivity persisted through 24 hours (Fig. 5D) and at least up to 48 hours (Fig. 5E) after the injection. Importantly, inhibiting NOX2 by i.c.v injection of GSK2795039 prior to $A\beta_{1-42}$ injection completely prevented network abnormalities at

all time points (Fig. 5B-E). This suggests that NOX2 activation is critical not only for $A\beta_{1-42}$-induced brain glucose hypometabolism, but also for $A\beta_{1-42}$-induced network bnormalities. This is in line with our previous reports showing that NOX2 is the primary trigger of epileptic seizures *(32)* and brain glucose hypometabolism-induced network hyperactivity and epileptogenesis *(27)*. It has previously been shown that Aβ-induced network dysfunction can lead to changes in mouse behavior profile *(47, 48)*. To evaluate a possible role of NOX2-induced oxidative stress in such neuropsychiatric-like disturbances, we performed exploratory experiments that revealed that inhibition of NOX2 by GSK2795039 prevented anxiety and aggression induced by i.c.v. $A\beta_{1-42}$ injection in mice (fig S1).

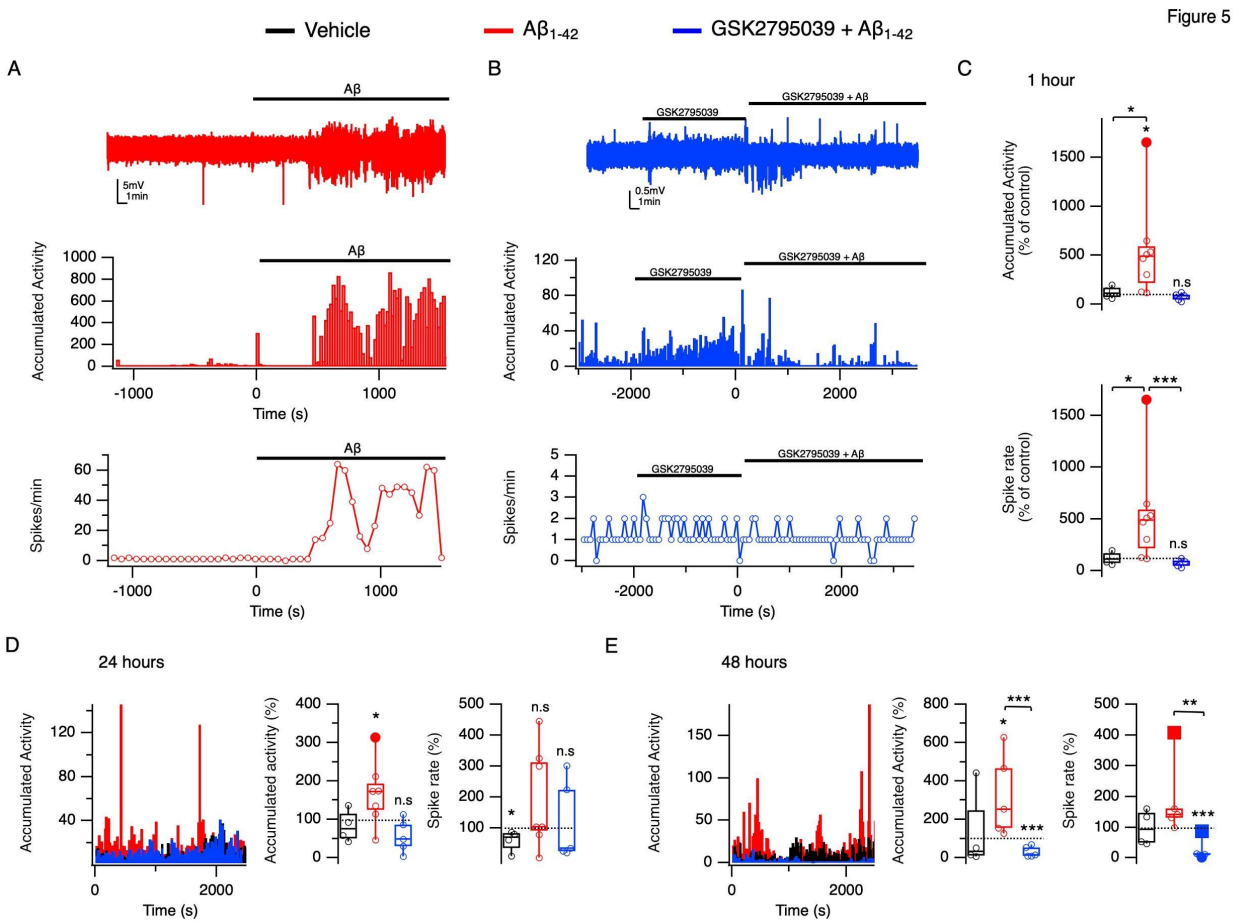

Figure 5. ***NOX2 mediates Aβ effect on network activity in-vivo.*** **A.** $A\beta_{1-42}$ i.c.v. injection results in an immediate increase in network activity and interictal spike frequency in awake freely moving mice. Top, example LFP trace from hippocampal CA1 stratum pyramidale before and after Aβ injection. Middle: accumulated activity integrals analyzed from the top trace. Bottom: interictal spike frequency analyzed from the top trace. **B.** NOX2 blockade prevents Aβ-induced hyperactivity. Top: example LFP trace from hippocampal CA1 stratum pyramidale in control, following GSK2795039 injection, and after subsequent Aβ injection. Middle: accumulated activity integrals analyzed from the top trace. Bottom: interictal spike frequency analyzed from the top trace. **C.** Mean accumulated activity integral and interictal spike frequency values for all acute experiments (n = 4 for vehicle group (black), n = 8 for Aβ group (red), and n = 6 for Aβ+GSK group (blue). **D.** Aβ-induced hyperactivity persists 24 hours following the Aβ injection and is prevented by preceding GSK2795039 application. Left, average accumulated activity for all recordings. Middle, average accumulated activity integrals. Right, average interictal spike frequency values. (n = 4 for vehicle group (black), n = 7 for Aβ group (red), and n = 6 for Aβ+GSK group (blue)). **E.** Aβ-induced hyperactivity persists 48 hours following the Aβ injection and is prevented by preceding GSK2795039 application. Left, average accumulated activity for all recordings. Middle, average accumulated activity integrals. Right, average interictal spike frequency values. (n = 4 for vehicle group (black), n = 7 for Aβ group (red) and n = 6 for Aβ+GSK group (blue)). *p<0.01, **p<0.02, *p<0.05

Discussion

Glucose hypometabolism is implicated in the initiation of sporadic AD, as it is associated with many AD risk factors *(10–13)*. Glucose hypometabolism occurs in patients with amnestic mild cognitive impairment (aMCI), widely thought to be a prodromal stage of AD *(10, 14, 15)*, and has also been detected in AD patients almost two decades prior to the onset of clinical symptoms.

Nevertheless, the mechanisms driving glucose hypometabolism and its relationship to cognitive decline have remained unclear. As a result, there are no approaches to prevent this pathology, and no understanding of how such intervention would impact disease progression. Importantly, brain hypometabolism in AD is always associated with oxidative stress (for review, *(12, 15)*). However, a causative link between these two factors, while hypothesized *(12)*, has never been demonstrated experimentally. Multiple studies have shown that oxidative stress during AD is largely induced by oligomeric Aβ, yet any relationship between Aβ-induced oxidative stress and glucose utilization has not been described. In this study, we report that oligomeric $A\beta_{1-42}$ impairs hippocampal glucose utilization via activation of neuronal NOX2 and the consequent oxidative stress. Shedding light on the causality between multiple AD-related pathologies, we show that inhibition of NOX2 with the selective antagonist GSK2795039 prevents the toxic effects of Aβ on glucose metabolism, network activity, and behavioral profile.

Glucose supports multiple critical cellular functions such as energy supply, antioxidant defense, and nucleotide biosynthesis *(16)*. Therefore, glucose hypometabolism can have many potentially harmful consequences, particularly energy shortages. Energy deficiency has been reported to result in BACE1 upregulation and increased production of Aβ *(19, 20)*. Accumulation of $A\beta_{1-42}$ is a key to the pathogenesis of AD and is known to induce oxidative stress *(17)*. We now show that Aβ also inhibits glucose utilization, thus establishing a vicious cycle of brain hypometabolism.

Acute application of oligomeric $A\beta_{1-42}$ resulted in a pronounced reduction of glucose utilization in hippocampal slices during network activity. *In vivo,* hippocampal i.c.v. administration of $A\beta_{1-42}$ induced a prominent increase in activity-driven extracellular glucose transients. The latter effect is more difficult to interpret, given the dynamic supply of glucose from the blood that increases to compensate for the energy demand from network activity. However, when considered together with the results from brain slices where the glucose supply is constant, the augmented extracellular glucose transients *in vivo* likely indicate decreased glucose consumption following $A\beta_{1-42}$

injection. Both *ex vivo* and *in vivo*, these effects of Aβ on glucose metabolism were mediated by oxidative stress, and could be completely prevented by blockade of NOX2 activity. These results define NOX2 as the enzyme largely responsible for the observed toxic effect(s) of $A\beta_{1-42}$. Indeed, in freely moving animals, we observed hippocampal electrical hyperactivity and abnormal animal behavior more than 48 hours after oligomeric $A\beta_{1-42}$ i.c.v. injection, confirming previous studies *(49, 50) (47, 51, 52)*. Crucially, pre-treating mice with i.c.v. injection of an NOX2 antagonist prevented these Aβ toxicities, suggesting that NOX2-induced oxidative stress may underlie not only brain hypometabolism but also major electrophysiological and behavioral deficits in preclinical AD. Thus, NOX2 is a promising therapeutic target for AD.

The NOX family of enzymes are transmembrane proteins that transport an electron from cytosolic NADPH to reduce oxygen to superoxide anion. There are seven known isoforms of NOX, with NOX1, NOX2 and NOX4 expressed in multiple brain regions including the cerebral cortex, hippocampus, cerebellum, hypothalamus, midbrain and/or striatum *(53)*. Of these NOX variants, NOX2 is the predominant form expressed by microglia, neurons, and astrocytes. Several lines of evidence including postmortem analyses of AD patient cerebral cortices indicate that oxidative stress—particularly resulting from NOX2 activation—plays a significant role in the development of AD *(23, 35, 36, 53, 54)*. The close relationship between the levels of Aβ and NOX2 activity has also been well documented in multiple studies *(22, 38, 55–59)*.

The selective NOX2 antagonist GSK2795039 that we used in our study is a novel small-molecule selective and direct inhibitor of NOX2 with brain bioavailability following systematic (oral) administration *(34)*. GSK2795039 was fully characterized in *in vivo* mouse paw inflammation models, which demonstrated the relationship between dosage, blood levels, and NOX2 enzyme inhibition over time *(34)*. GSK2795039 is presumably not cytotoxic at the concentrations used for NOX2 inhibition *(34)*: it was well tolerated in rodents, with no obvious adverse effects following 5 days of twice-daily dosing *(34)*. Following oral administration, GSK2795039 was detected in

the blood and the central nervous system, indicating that it can cross the blood-brain barrier *(34)*. Thus to our knowledge, GSK2795039 is the only available selective NOX2 inhibitor that may be appropriate for the development of future AD therapies *(60)*.

Oxidative stress can induce multiple and multi-factorial damage in the brain, as ROS damage DNA, lipids and proteins, ultimately resulting in necrosis and apoptotic cell death *(12, 61)*. Glucose hypometabolism can also result in multiple impairments. We show that NOX2-induced oxidative stress is actually the direct cause of deficient glucose metabolism. Thus, the question is whether the network and behavioral pathologies we observed in our study can be explained by glucose hypometabolism alone, by oxidative stress, or by some combination of both. This is challenging to resolve since in most cases oxidative stress and hypometabolism occur in synergy and in a feedback loop. We showed previously that acute application of H_2O_2 induced a long-lasting reduction in glucose utilization and decreased synaptic transmission *(31)*. On the other hand, we have also found that partial inhibition of brain glucose utilization by chronic i.c.v. administration of 2-DG induced hyperactivity and epileptogenesis *in vivo (27)*. However, we cannot rule out the possibility that secondary NOX activation resulting from glucose hypometabolism causes hyperactivity, forming yet another oxidative stress – hypometabolism – network dysfunction positive feedback loop. In any case, in the present study, we establish a direct causal link between NOX2 activity and glucose utilization, and show that NOX2 inhibition with consequent prevention of glucose hypometabolism is sufficient to ameliorate many Aβ-induced downstream pathologies, including behavioral deficits.

Given the primary role of oxidative stress in AD pathology, one potential treatment strategy could be scavenging ROS by antioxidants. However, clinical trials in aMCI and AD patients using antioxidants have so far been disappointing *(12, 62)*. Our previous studies might provide an explanation for this apparent discrepancy. Using an amperometric technique to detect extracellular H_2O_2 transients evoked by interictal activity in hippocampal slices, we recorded the dynamic

release of ROS from a network of synchronously activated cells *(31, 32)*. We showed that the potent antioxidant Tempol *(63, 64)*, even at high concentrations of 4 mM, did not reduce the transient amplitude of NOX-derived H_2O_2 "spike" by more than 20% *(31),* and failed to abate rapid ROS accumulation resulting from NOX2 activation during epileptic seizures *(32)*. Therefore, it may be that oral administration of antioxidants cannot achieve the brain antioxidant levels necessary to mediate the oxidative stress induced by NOX activation.

Intriguingly, glucose hypometabolism is also a prominent feature of epilepsy, and we have shown recently that glucose utilization deficiency can be induced by just a few epileptic seizures *(31)*. Moreover, we found that seizure onset is dependent on rapid ROS release from NOX2 activation *(32)*. Notably, just as with AD, the major risk factors for acquired epilepsy are associated with oxidative stress and glucose hypometabolism *(18, 65, 66)*. Multiple studies in rodent epilepsy models have demonstrated that reduced glucose metabolism is predictive of disease initiation *(67)*. Therefore, the combination of oxidative stress and glucose hypometabolism may be a primary mechanism underlying epilepsy progression *(65)*. Moreover, oxidative stress, neuroinflammation, and hypometabolism acting in concert, particularly NOX-induced oxidative stress, have been reported in the early stages of other major neurodegenerative diseases *(18, 61, 68, 69)(23, 70)*. Therefore, we posit that the role of NOX-hypometabolism axis is pervasive in neurodegenerative disease initiation, and special attention should be paid to NOX2 in the search for effective treatments.

In the brain, NOX2 is largely expressed in microglia, the resident brain phagocytes, where it is used as a host defense mechanism. However, our experiments suggest that neurons play the dominant role in producing $A\beta_{1-42}$- induced ROS toxicity. While NOX2 in microglia is activated in response to neurotoxic stimulation *(54)*, NMDA receptor stimulation is required for NOX2 activation in neurons *(39)*, and we found that blockade of NMDARs by APV recapitulated the effect of NOX2 inhibition. Importantly, we cannot rule out a possible contribution of microglia,

as the expression of NMDARs has been reported for microglia *(71)*, although the presence of functional microglial NMDARs *in situ* is a matter of debate *(72, 73)* and our microglial depletion experiments did not achieve complete ablation. Further experiments will also be needed to evaluate a potential contribution of astrocytes, which express both NMDARs and NOX.

In summary, in this study we established a link between $A\beta_{1-42}$, NOX2-induced oxidative stress, glucose hypometabolism, and network hyperactivity in AD pathogenesis. We also demonstrate a potency of selective NOX2 inhibitor GSK2795039 in preventing toxic $A\beta_{1-42}$ effects, and propose NOX2 as a primary target for early interventions in Alzheimer's disease, which warrants further studies.

Materials and Methods

All animal protocols and experimental procedures were approved by the Ethics Committees for Animal Experimentation at the INSERM (#30-03102012), ITEB RAS, the University of California, and Gladstone Institutes under IACUC protocol AN176773.

Ex vivo experiments

Tissue slice preparation

Recordings were performed on brain slices from P21-56 OF1 male mice (Charles River Laboratories, France) or C57/Bl6 mice (Jackson Labs, USA). Mice anaesthetized with isoflurane were decapitated; the brain was rapidly removed from the skull and placed in the ice-cold ACSF. The ACSF solution consisted of (in mmol/L): NaCl 126, KCl 3.50, NaH_2PO_4 1.25, $NaHCO_3$ 25, $CaCl_2$ 2.00, $MgCl_2$ 1.30, and dextrose 5, pH 7.4. ACSF was aerated with 95% O2/5% CO_2 gas mixture. Sagittal slices (350 μm) were cut using a tissue slicer (Leica VT 1200s, Leica Microsystem, Germany). During cutting, slices were submerged in an ice-cold (< 6°C) solution consisting of (in mmol/L): K-gluconate 140, HEPES 10, Na-gluconate 15, EGTA 0.2, NaCl 4, pH

adjusted to 7.2 with KOH. Slices were immediately transferred to a multi-section, dual-side perfusion holding chamber with constantly circulating ACSF and allowed to recover for 2h at room temperature (22°C-24°C).

Synaptic stimulation and field potential recordings

Slices were transferred to a recording chamber continuously superfused (10 ml/min) with ACSF (33–34°C) with access to both slice sides. Schaffer collateral/commissures was stimulated using the DS2A isolated stimulator (Digitimer Ltd, UK) with a bipolar metal electrode. Stimulus current was adjusted using single pulses (40-170 µA, 200µs, 0.15 Hz) to induce a LFP of about 50% maximal amplitude. LFPs were recorded using glass microelectrodes filled with ASCF, placed in stratum pyramidale of CA1 area and connected to the ISO DAM-8A amplifier (WPI, FL). Synaptic stimulation consisted of a stimulus train (200µs pulses) at 100 Hz lasting 1s.

Oxygen and glucose measurements

A Clark-style oxygen microelectrode (Unisense Ltd, Denmark) was used to measure slice tissue pO_2. Extracellular glucose was measured using enzymatic microelectrodes (Sarissa Biomedical, Coventry, UK) connected to a free radical analyzer TBR4100 (Word Precision Instruments Ltd, UK).

NAD(P)H fluorescence imaging.

Changes in NAD(P)H autofluorescence in hippocampal slices were recorded as described previously *(28)*. Data were expressed as the percentage change in fluorescence over baseline [(DF/F) · 100].

Pharmacology

Antagonist of NMDA receptors, (2R)-amino-5-phosphonopentanoate (APV) was purchased from Tocris Bioscience (Bio-Techne Ltd, UK); GSK2795039 from MedChemExpress.

In vivo experiments on freely-moving animals

Animals and surgery

Eighteen CD-1 mature male mice (35- 45g) were used for in vivo experiments. Before the experiment mice were implanted with nichrome recording electrodes in the CA1 (AP=-2.5mm, ML= 2mm, H=1.5mm) and dentate gyrus (AP=-2mm, ML= 0.8mm, H=2.5mm), and a guide cannula for i.c.v. injections (AP=-0.2mm, ML= 1.8mm, H=2.2mm). Animals were anesthetized with Zoletil (120 mg/kg) supplemented with xylazine (10mg/kg). Electrode and cannula placements were verified post-mortem. An indifferent electrode was screwed into the occipital bone.

Drug administration

Animals received either 1µl vehicle (NaCl 0.9%+PBS+Glucose 5mM) or 1µl of $A\beta_{1-42}$ (Sigma-Aldrich, 4mg/ml in 1.0% NH_4OH) intracerebroventricularly (i.c.v.) using a Hamilton syringe. In experiments with GSK2795039, 1µl of inhibitor solution (20mg/ml) was injected 30 min prior to $A\beta_{1-42}$ and additionally 1µl together with $A\beta_{1-42}$ solution.

LFP recordings

After a four-day recovery period, LFP recordings on freely-moving animals were initiated. Following 60-minute recordings of control activity, animals received an injection of the appropriate drug. To estimate acute effects, brain activity was monitored 90 min after drug application. For the 3 days following the experiment, animals received daily i.c.v. injection of either vehicle (control and Aβ groups) or GSK2795039 (Aβ+GSK group). 1-hour long LFP recordings were performed 24h and 48h after the acute experiments.

LFPs were filtered (high-pass filter 0.1Hz, low-pass filter 5kHz) and recorded at 10kHz sampling rate. Each recording was normalized to its own baseline activity (SD). Accumulated activity integrals and interictal spikes were detected as described previously *(27, 46)* using custom macros in IgorPro (Wavemetrics, USA). Briefly, accumulated activity constitutes a sum of all events

exceeding the 3xSD threshold and binned at 20sec intervals. Interictal spikes were detected as any event exceeding 3xSD amplitude and lasting between 10-990msec.

In vivo experiments on anesthetized animals

Animals and surgery

For acute glucose measurements, animals (n=6) were anesthetized with pentobarbital (60mg/kg) supplemented with xylazine (20 mg/kg). Animals were placed in a stereotaxic frame, scalped, and holes for electrodes and guide cannula were drilled. In addition to hippocampal field electrode and guide cannula, a bipolar stimulating electrode was implanted to the fimbria fornix (AP=-0.4mm, L= 1mm, H=3mm, approach angle 15°) for hippocampal network activation. A cranial window (Ø 1.5mm) above the hippocampus was drilled ipsilateral to the cannula, and a Sarissa glucose sensor was dipped in the hippocampus (2mm) using a micromanipulator. After surgical preparation, the cortex was kept under saline to prevent drying.

LFPs and extracellular glucose measurement

LFPs and extracellular glucose were measured using the same equipment used for in vitro experiments. Following 2-3 stimulations in control conditions, Aβ1-42 or GSK2795039 were injected prior to Aβ1-42.

PLX treatment

To deplete microglia, mice were switched to PLX5622 diet (PLX5622-enriched chow was provided by Research Diets, Inc., New Brunswick, USA). Mice were on the ad libitum diet for 7-15 days. Approximately 5 mg of PLX5622 was ingested daily by mice of 35 grams of weight.

Histological analysis

Free-floating slices (35 μm) from perfused animals were incubated with Triton X (0.3%) in PBS three times for 5 min, followed by blocking solution (BSA 1%, Triton X 0.3% in PBS) for 2 h. Then, the primary antibody rabbit anti-Iba-1 (1:1000; Wako, Japan) was added and slices were incubated overnight at 4◦C. Next day, the secondary antibodies goat anti-rabbit (1:1000; Alexa Fluor 488, ThermoFisher, USA) were added for 2 h. After washout in PBS with 0.3% TritonX-100, slices were mounted on gelatinized covers in Fluoromount media (Sigma-Aldrich, USA). Immunostaining was analyzed under a Nikon E200 fluorescence microscope. In order to make a proper comparison, equivalent regions containing similar portions were chosen for all the groups. 3+ sections per animal were used for averaging. Photomicrographs using 10X (0.25 of numerical aperture) of stained fluorescence were quantified with the aid of ImageJ software (NIH, USA), and the whole hippocampus was used for quantification. The number of Iba-1+cells and % total labelled area was calculated.

Drug administration

A guide cannula (stainless steel, 21 gauge) was implanted above the left lateral brain ventricle (AP = –0.7; L = 1.37; H = 1.25). Drugs were administered 1-month post-surgery to avoid surgery side effects. Mice were allocated to three groups: control (n = 6), Aβ (n = 5), and Aβ+GSK2795039 (n = 6). Injections were made i.c.v. through the guide cannula (1 μl/min) to awake mice. All substances were injected in equal volumes (1 μl) and the guide cannula was closed by a plunger. Mice in the Aβ+GSK2795039 group received GSK2795039 (MedChemExpress Europe; 4.5 mg/ml in DMSO)-and $A\beta_{1-42}$ (Sigma-Aldrich, 4mg/ml in 1.0% NH_4OH) on the first day, and daily GSK2795039 further for 14 days. Mice in the Aβ group received $A\beta_{1-42}$ on the first day, and daily DMSO further for 14 days. Mice in the control group received daily DMSO for 15 days.

Statistical analysis

Paired experiments were analyzed by Student's t-test; group comparisons were made using the Kruskal-Wallis test, Mann-Whitney U test or one-way ANOVA, where appropriate. Data are presented as mean ± SEM.

List of Supplementary Materials

Supplementary Figure 1, Supplementary methods

References

1. B. Dubois, H. Hampel, H. H. Feldman, P. Scheltens, P. Aisen, S. Andrieu, H. Bakardjian, H. Benali, L. Bertram, K. Blennow, K. Broich, E. Cavedo, S. Crutch, J.-F. Dartigues, C. Duyckaerts, S. Epelbaum, G. B. Frisoni, S. Gauthier, R. Genthon, A. A. Gouw, M.-O. Habert, D. M. Holtzman, M. Kivipelto, S. Lista, J.-L. Molinuevo, S. E. O'Bryant, G. D. Rabinovici, C. Rowe, S. Salloway, L. S. Schneider, R. Sperling, M. Teichmann, M. C. Carrillo, J. Cummings, C. R. Jack Jr, Proceedings of the Meeting of the International Working Group (IWG) and the American Alzheimer's Association on "The Preclinical State of AD"; July 23, 2015; Washington DC, USA, Preclinical Alzheimer's disease: Definition, natural history, and diagnostic criteria, *Alzheimers. Dement.* **12**, 292–323 (2016).

2. A. Lloret, D. Esteve, M.-A. Lloret, A. Cervera-Ferri, B. Lopez, M. Nepomuceno, P. Monllor, When Does Alzheimer's Disease Really Start? The Role of Biomarkers, *Int. J. Mol. Sci.* **20** (2019), doi:10.3390/ijms20225536.

3. C. R. Jack Jr, D. A. Bennett, K. Blennow, M. C. Carrillo, B. Dunn, S. B. Haeberlein, D. M. Holtzman, W. Jagust, F. Jessen, J. Karlawish, E. Liu, J. L. Molinuevo, T. Montine, C. Phelps, K. P. Rankin, C. C. Rowe, P. Scheltens, E. Siemers, H. M. Snyder, R. Sperling, Contributors, NIA-AA Research Framework: Toward a biological definition of Alzheimer's disease, *Alzheimers. Dement.* **14**, 535–562 (2018).

4. E. N. Cline, M. A. Bicca, K. L. Viola, W. L. Klein, The Amyloid-β Oligomer Hypothesis: Beginning of the Third Decade, *J. Alzheimers. Dis.* **64**, S567–S610 (2018).

5. T. Guo, D. Korman, S. L. Baker, S. M. Landau, W. J. Jagust, Longitudinal cognitive and biomarker measurements support a unidirectional pathway in Alzheimer's Disease pathophysiology, *Biol. Psychiatry* (2020), doi:10.1016/j.biopsych.2020.06.029.

6. B. Penke, M. Szűcs, F. Bogár, Oligomerization and Conformational Change Turn Monomeric β-Amyloid and Tau Proteins Toxic: Their Role in Alzheimer's Pathogenesis, *Molecules* **25** (2020), doi:10.3390/molecules25071659.

7. A. Clement, O. Wiborg, A. A. Asuni, Steps Towards Developing Effective Treatments for Neuropsychiatric Disturbances in Alzheimer's Disease: Insights From Preclinical Models, Clinical Data, and Future Directions, *Front. Aging Neurosci.* **12**, 56 (2020).

8. K. P. Ng, T. A. Pascoal, S. Mathotaarachchi, C.-O. Chung, A. L. Benedet, M. Shin, M. S. Kang, X. Li, M. Ba, N. Kandiah, P. Rosa-Neto, S. Gauthier, Alzheimer's Disease Neuroimaging Initiative,

Neuropsychiatric symptoms predict hypometabolism in preclinical Alzheimer disease, *Neurology* **88**, 1814–1821 (2017).

9. N. Goukasian, K. S. Hwang, T. Romero, J. Grotts, T. M. Do, J. R. Groh, D. R. Bateman, L. G. Apostolova, Association of brain amyloidosis with the incidence and frequency of neuropsychiatric symptoms in ADNI: a multisite observational cohort study, *BMJ Open* **9**, e031947 (2019).

10. S. P. Caminiti, T. Ballarini, A. Sala, C. Cerami, L. Presotto, R. Santangelo, F. Fallanca, E. G. Vanoli, L. Gianolli, S. Iannaccone, G. Magnani, D. Perani, BIOMARKAPD Project, FDG-PET and CSF biomarker accuracy in prediction of conversion to different dementias in a large multicentre MCI cohort, *Neuroimage Clin* **18**, 167–177 (2018).

11. B. A. Gordon, T. M. Blazey, Y. Su, A. Hari-Raj, A. Dincer, S. Flores, J. Christensen, E. McDade, G. Wang, C. Xiong, N. J. Cairns, J. Hassenstab, D. S. Marcus, A. M. Fagan, C. R. Jack Jr, R. C. Hornbeck, K. L. Paumier, B. M. Ances, S. B. Berman, A. M. Brickman, D. M. Cash, J. P. Chhatwal, S. Correia, S. Förster, N. C. Fox, N. R. Graff-Radford, C. la Fougère, J. Levin, C. L. Masters, M. N. Rossor, S. Salloway, A. J. Saykin, P. R. Schofield, P. M. Thompson, M. M. Weiner, D. M. Holtzman, M. E. Raichle, J. C. Morris, R. J. Bateman, T. L. S. Benzinger, Spatial patterns of neuroimaging biomarker change in individuals from families with autosomal dominant Alzheimer's disease: a longitudinal study, *Lancet Neurol.* **17**, 241–250 (2018).

12. D. A. Butterfield, B. Halliwell, Oxidative stress, dysfunctional glucose metabolism and Alzheimer disease, *Nat. Rev. Neurosci.* **20**, 148–160 (2019).

13. T. Wisniewski, Ed., *Alzheimer's Disease* (Codon Publications, Brisbane (AU), 2020).

14. A. Drzezga, N. Lautenschlager, H. Siebner, M. Riemenschneider, F. Willoch, S. Minoshima, M. Schwaiger, A. Kurz, Cerebral metabolic changes accompanying conversion of mild cognitive impairment into Alzheimer's disease: a PET follow-up study, *Eur. J. Nucl. Med. Mol. Imaging* **30**, 1104–1113 (2003).

15. L. Mosconi, A. Pupi, M. J. De Leon, Brain glucose hypometabolism and oxidative stress in preclinical Alzheimer's disease, *Ann. N. Y. Acad. Sci.* **1147**, 180–195 (2008).

16. G. A. Dienel, Brain Glucose Metabolism: Integration of Energetics with Function, *Physiol. Rev.* **99**, 949–1045 (2019).

17. D. A. Butterfield, D. Boyd-Kimball, Oxidative Stress, Amyloid-β Peptide, and Altered Key Molecular Pathways in the Pathogenesis and Progression of Alzheimer's Disease, *J. Alzheimers. Dis.* **62**, 1345–1367 (2018).

18. Y. Zilberter, M. Zilberter, The vicious circle of hypometabolism in neurodegenerative diseases: Ways and mechanisms of metabolic correction, *J. Neurosci. Res.* **95**, 2217–2235 (2017).

19. R. A. Velliquette, T. O'Connor, R. Vassar, Energy inhibition elevates beta-secretase levels and activity and is potentially amyloidogenic in APP transgenic mice: possible early events in Alzheimer's disease pathogenesis, *Journal of Neuroscience* **25**, 10874–10883 (2005).

20. T. O'Connor, K. R. Sadleir, E. Maus, R. A. Velliquette, J. Zhao, S. L. Cole, W. A. Eimer, B. Hitt, L. A. Bembinster, S. Lammich, S. F. Lichtenthaler, S. S. Hébert, B. De Strooper, C. Haass, D. A. Bennett, R. Vassar, Phosphorylation of the translation initiation factor eIF2alpha increases BACE1 levels and promotes amyloidogenesis, *Neuron* **60**, 988–1009 (2008).

21. C. Cheignon, M. Tomas, D. Bonnefont-Rousselot, P. Faller, C. Hureau, F. Collin, Oxidative stress and the amyloid beta peptide in Alzheimer's disease, *Redox Biol* **14**, 450–464 (2018).

22. P. B. Shelat, M. Chalimoniuk, J.-H. Wang, J. B. Strosznajder, J. C. Lee, A. Y. Sun, A. Simonyi, G. Y. Sun, Amyloid beta peptide and NMDA induce ROS from NADPH oxidase and AA release from cytosolic phospholipase A2 in cortical neurons, *J. Neurochem.* **106**, 45–55 (2008).

23. A. Tarafdar, G. Pula, The Role of NADPH Oxidases and Oxidative Stress in Neurodegenerative Disorders, *Int. J. Mol. Sci.* **19** (2018), doi:10.3390/ijms19123824.

24. A. Y. Abramov, E. V. Potapova, V. V. Dremin, A. V. Dunaev, Interaction of Oxidative Stress and Misfolded Proteins in the Mechanism of Neurodegeneration, *Life* **10** (2020), doi:10.3390/life10070101.

25. M. Zilberter, A. Ivanov, S. Ziyatdinova, M. Mukhtarov, A. Malkov, A. Alpar, G. Tortoriello, C. H. Botting, L. Fulop, A. A. Osypov, A. Pitkanen, H. Tanila, T. Harkany, Y. Zilberter, Dietary energy substrates reverse early neuronal hyperactivity in a mouse model of Alzheimer's disease, *J. Neurochem.* **125**, 157–171 (2013).

26. E. A. Kiyatkin, M. Lenoir, Rapid fluctuations in extracellular brain glucose levels induced by natural arousing stimuli and intravenous cocaine: fueling the brain during neural activation, *J. Neurophysiol.* **108**, 1669–1684 (2012).

27. E. Samokhina, I. Popova, A. Malkov, A. I. Ivanov, D. Papadia, A. Osypov, M. Molchanov, S. Paskevich, A. Fisahn, M. Zilberter, Y. Zilberter, Chronic inhibition of brain glycolysis initiates epileptogenesis, *J. Neurosci. Res.* **95**, 2195–2206 (2017).

28. A. I. Ivanov, A. E. Malkov, T. Waseem, M. Mukhtarov, S. Buldakova, O. Gubkina, M. Zilberter, Y. Zilberter, Glycolysis and oxidative phosphorylation in neurons and astrocytes during network activity in hippocampal slices, *J. Cereb. Blood Flow Metab.* **34**, 397–407 (2014).

29. R. H. Swerdlow, L. E, D. Aires, J. Lu, Glycolysis-respiration relationships in a neuroblastoma cell line, *Biochim. Biophys. Acta* **1830**, 2891–2898 (2013).

30. F. Galeffi, P. K. Shetty, M. P. Sadgrove, D. A. Turner, Age-related metabolic fatigue during low glucose conditions in rat hippocampus, *Neurobiol. Aging* **36**, 982–992 (2015).

31. A. Malkov, A. I. Ivanov, S. Buldakova, T. Waseem, I. Popova, M. Zilberter, Y. Zilberter, Seizure-induced reduction in glucose utilization promotes brain hypometabolism during epileptogenesis, *Neurobiol. Dis.* **116**, 28–38 (2018).

32. A. Malkov, A. I. Ivanov, A. Latyshkova, P. Bregestovski, M. Zilberter, Y. Zilberter, Activation of nicotinamide adenine dinucleotide phosphate oxidase is the primary trigger of epileptic seizures in rodent models, *Ann. Neurol.* **85**, 907–920 (2019).

33. T. E. Decoursey, E. Ligeti, Regulation and termination of NADPH oxidase activity, *Cell. Mol. Life Sci.* **62**, 2173–2193 (2005).

34. K. Hirano, W. S. Chen, A. L. Chueng, A. A. Dunne, T. Seredenina, A. Filippova, S. Ramachandran, A. Bridges, L. Chaudry, G. Pettman, C. Allan, S. Duncan, K. C. Lee, J. Lim, M. T. Ma, A. B. Ong, N. Y. Ye, S. Nasir, S. Mulyanidewi, C. C. Aw, P. P. Oon, S. Liao, D. Li, D. G. Johns, N. D. Miller, C. H. Davies, E. R. Browne, Y. Matsuoka, D. W. Chen, V. Jaquet, A. R. Rutter, Discovery of GSK2795039, a Novel Small Molecule NADPH Oxidase 2 Inhibitor, *Antioxid. Redox Signal.* **23**, 358–374 (2015).

35. S. Sorce, R. Stocker, T. Seredenina, R. Holmdahl, A. Aguzzi, A. Chio, A. Depaulis, F. Heitz, P. Olofsson, T. Olsson, V. Duveau, D. Sanoudou, S. Skosgater, A. Vlahou, D. Wasquel, K.-H. Krause, V. Jaquet, NADPH oxidases as drug targets and biomarkers in neurodegenerative diseases: What is

the evidence?, *Free Radic. Biol. Med.* **112**, 387–396 (2017).

36. M. W. Ma, J. Wang, Q. Zhang, R. Wang, K. M. Dhandapani, R. K. Vadlamudi, D. W. Brann, NADPH oxidase in brain injury and neurodegenerative disorders, *Mol. Neurodegener.* **12**, 7 (2017).

37. A. M. Brennan-Minnella, S. J. Won, R. A. Swanson, NADPH oxidase-2: linking glucose, acidosis, and excitotoxicity in stroke, *Antioxid. Redox Signal.* **22**, 161–174 (2015).

38. A. Y. Abramov, M. R. Duchen, The role of an astrocytic NADPH oxidase in the neurotoxicity of amyloid beta peptides, *Philos. Trans. R. Soc. Lond. B Biol. Sci.* **360**, 2309–2314 (2005).

39. A. M. Minnella, J. X. Zhao, X. Jiang, E. Jakobsen, F. Lu, L. Wu, J. El-Benna, J. A. Gray, R. A. Swanson, Excitotoxic superoxide production and neuronal death require both ionotropic and non-ionotropic NMDA receptor signaling, *Sci. Rep.* **8**, 17522 (2018).

40. Y. Liu, K. S. Given, E. L. Dickson, G. P. Owens, W. B. Macklin, J. L. Bennett, Concentration-dependent effects of CSF1R inhibitors on oligodendrocyte progenitor cells ex vivo and in vivo, *Exp. Neurol.* **318**, 32–41 (2019).

41. N. N. Dagher, A. R. Najafi, K. M. N. Kayala, M. R. P. Elmore, T. E. White, R. Medeiros, B. L. West, K. N. Green, Colony-stimulating factor 1 receptor inhibition prevents microglial plaque association and improves cognition in 3xTg-AD mice, *J. Neuroinflammation* **12**, 139 (2015).

42. K. A. Vossel, M. C. Tartaglia, H. B. Nygaard, A. Z. Zeman, B. L. Miller, Epileptic activity in Alzheimer's disease: causes and clinical relevance, *Lancet Neurol.* **16**, 311–322 (2017).

43. K. A. Vossel, A. J. Beagle, G. D. Rabinovici, H. Shu, S. E. Lee, G. Naasan, M. Hegde, S. B. Cornes, M. L. Henry, A. B. Nelson, W. W. Seeley, M. D. Geschwind, M. L. Gorno-Tempini, T. Shih, H. E. Kirsch, P. A. Garcia, B. L. Miller, L. Mucke, Seizures and epileptiform activity in the early stages of Alzheimer disease, *JAMA Neurol.* **70**, 1158–1166 (2013).

44. M. A. Busche, A. Konnerth, Impairments of neural circuit function in Alzheimer's disease, *Philos. Trans. R. Soc. Lond. B Biol. Sci.* **371** (2016), doi:10.1098/rstb.2015.0429.

45. R. Minkeviciene, S. Rheims, M. B. Dobszay, M. Zilberter, J. Hartikainen, L. Fülöp, B. Penke, Y. Zilberter, T. Harkany, A. Pitkänen, H. Tanila, Fibrillar β-amyloid-induced hyperexcitability of cortical and hippocampal neurons triggers progressive epilepsy, *J. Neurosci.* **29**, 3453–3462 (2009).

46. I. Popova, A. Malkov, A. I. Ivanov, E. Samokhina, S. Buldakova, O. Gubkina, A. Osypov, R. S. Muhammadiev, T. Zilberter, M. Molchanov, S. Paskevich, M. Zilberter, Y. Zilberter, Metabolic correction by pyruvate halts acquired epilepsy in multiple rodent models, *Neurobiol. Dis.* **106**, 244–254 (2017).

47. S. Sharma, S. Verma, M. Kapoor, A. Saini, B. Nehru, Alzheimer's disease like pathology induced six weeks after aggregated amyloid-beta injection in rats: increased oxidative stress and impaired long-term memory with anxiety-like behavior, *Neurol. Res.* **38**, 838–850 (2016).

48. S. Sharma, N. Sharma, A. Saini, B. Nehru, Carbenoxolone Reverses the Amyloid Beta 1-42 Oligomer-Induced Oxidative Damage and Anxiety-Related Behavior in Rats, *Neurotox. Res.* **35**, 654–667 (2019).

49. D. Alcantara-Gonzalez, B. Villasana-Salazar, F. Peña-Ortega, Single amyloid-beta injection exacerbates 4-aminopyridine-induced seizures and changes synaptic coupling in the hippocampus, *Hippocampus* **29**, 1150–1164 (2019).

50. H. Chung, K. Park, H. J. Jang, M. M. Kohl, J. Kwag, Dissociation of somatostatin and parvalbumin interneurons circuit dysfunctions underlying hippocampal theta and gamma oscillations impaired by amyloid β oligomers in vivo, *Brain Struct. Funct.* (2020), doi:10.1007/s00429-020-02044-3.

51. C. Balducci, M. Beeg, M. Stravalaci, A. Bastone, A. Sclip, E. Biasini, L. Tapella, L. Colombo, C. Manzoni, T. Borsello, R. Chiesa, M. Gobbi, M. Salmona, G. Forloni, Synthetic amyloid-β oligomers impair long-term memory independently of cellular prion protein, *Proc. Natl. Acad. Sci. U. S. A.* **107**, 2295–2300 (2010).

52. S. Schmid, B. Jungwirth, V. Gehlert, M. Blobner, G. Schneider, S. Kratzer, K. Kellermann, G. Rammes, Intracerebroventricular injection of beta-amyloid in mice is associated with long-term cognitive impairment in the modified hole-board test*Behavioural Brain Research* **324**, 15–20 (2017).

53. L. Hou, L. Zhang, J.-S. Hong, D. Zhang, J. Zhao, Q. Wang, Nicotinamide Adenine Dinucleotide Phosphate Oxidase and Neurodegenerative Diseases: Mechanisms and Therapy, *Antioxid. Redox Signal.* (2020), doi:10.1089/ars.2019.8014.

54. R. Rastogi, X. Geng, F. Li, Y. Ding, NOX Activation by Subunit Interaction and Underlying Mechanisms in Disease, *Front. Cell. Neurosci.* **10**, 301 (2016).

55. L. Geng, L. M. Fan, F. Liu, C. Smith, J.-M. Li, Nox2 dependent redox-regulation of microglial response to amyloid-β stimulation and microgliosis in aging, *Sci. Rep.* **10**, 1582 (2020).

56. A. Wyssenbach, T. Quintela, F. Llavero, J. L. Zugaza, C. Matute, E. Alberdi, Amyloid β-induced astrogliosis is mediated by β1-integrin via NADPH oxidase 2 in Alzheimer's disease, *Aging Cell* **15**, 1140–1152 (2016).

57. R. Abeti, A. Y. Abramov, M. R. Duchen, Beta-amyloid activates PARP causing astrocytic metabolic failure and neuronal death, *Brain* **134**, 1658–1672 (2011).

58. R. O. Costa, P. N. Lacor, I. L. Ferreira, R. Resende, Y. P. Auberson, W. L. Klein, C. R. Oliveira, A. C. Rego, C. M. F. Pereira, Endoplasmic reticulum stress occurs downstream of GluN2B subunit of N-methyl-D-aspartate receptor in mature hippocampal cultures treated with amyloid-β oligomers, *Aging Cell* **11**, 823–833 (2012).

59. K. P. Walsh, L. S. Minamide, S. J. Kane, A. E. Shaw, D. R. Brown, B. Pulford, M. D. Zabel, J. D. Lambeth, T. B. Kuhn, J. R. Bamburg, Amyloid-β and proinflammatory cytokines utilize a prion protein-dependent pathway to activate NADPH oxidase and induce cofilin-actin rods in hippocampal neurons, *PLoS One* **9**, e95995 (2014).

60. F. Augsburger, A. Filippova, D. Rasti, T. Seredenina, M. Lam, G. Maghzal, Z. Mahiout, P. Jansen-Dürr, U. G. Knaus, J. Doroshow, R. Stocker, K.-H. Krause, V. Jaquet, Pharmacological characterization of the seven human NOX isoforms and their inhibitors, *Redox Biol* **26**, 101272 (2019).

61. A. Singh, R. Kukreti, L. Saso, S. Kukreti, Oxidative Stress: A Key Modulator in Neurodegenerative Diseases, *Molecules* **24** (2019), doi:10.3390/molecules24081583.

62. F. Pohl, P. Kong Thoo Lin, The Potential Use of Plant Natural Products and Plant Extracts with Antioxidant Properties for the Prevention/Treatment of Neurodegenerative Diseases: In Vitro, In Vivo and Clinical Trials, *Molecules* **23** (2018), doi:10.3390/molecules23123283.

63. C. S. Wilcox, Effects of tempol and redox-cycling nitroxides in models of oxidative stress, *Pharmacol. Ther.* **126**, 119–145 (2010).

64. P. Dohare, M. C. Hyzinski-Garcia, A. Vipani, N. H. Bowens, J. W. Nalwalk, P. J. Feustel, R. W. Keller Jr., D. Jourd'heuil, A. A. Mongin, The neuroprotective properties of the superoxide dismutase mimetic tempol correlate with its ability to reduce pathological glutamate release in a rodent model of stroke, *Free Radic. Biol. Med.* **77**, 168–182 (2014).

65. M. Patel, A Metabolic Paradigm for Epilepsy, *Epilepsy Curr.* **18**, 318–322 (2018).

66. J. N. Pearson-Smith, M. Patel, Metabolic Dysfunction and Oxidative Stress in Epilepsy, *Int. J. Mol. Sci.* **18** (2017), doi:10.3390/ijms18112365.

67. C. A. Reid, S. Mullen, T. H. Kim, S. Petrou, Epilepsy, energy deficiency and new therapeutic approaches including diet, *Pharmacol. Ther.* **144**, 192–201 (2014).

68. V. R. Muddapu, S. A. P. Dharshini, V. S. Chakravarthy, M. M. Gromiha, Neurodegenerative Diseases - Is Metabolic Deficiency the Root Cause?, *Front. Neurosci.* **14**, 213 (2020).

69. B. L. Tang, Glucose, glycolysis, and neurodegenerative diseases, *J. Cell. Physiol.* (2020), doi:10.1002/jcp.29682.

70. S. Barua, J. Y. Kim, M. A. Yenari, J. E. Lee, The role of NOX inhibitors in neurodegenerative diseases, *IBRO Rep* **7**, 59–69 (2019).

71. A. M. Kaindl, V. Degos, S. Peineau, E. Gouadon, Activation of microglial N- methyl- D-aspartate receptors triggers inflammation and neuronal cell death in the developing and mature brain, *Annals of* (2012) (available at https://onlinelibrary.wiley.com/doi/abs/10.1002/ana.23626).

72. U. B. Eyo, L.-J. Wu, Microglia: Lifelong patrolling immune cells of the brain, *Prog. Neurobiol.* **179**, 101614 (2019).

73. S. Wendt, E. Wogram, L. Korvers, H. Kettenmann, Experimental Cortical Spreading Depression Induces NMDA Receptor Dependent Potassium Currents in Microglia, *J. Neurosci.* **36**, 6165–6174 (2016).

Acknowledgments:

This study was supported by the National Institute on Aging grant R01AG061150 to MZ, RSF grants #17-75-20245 to AM and #20-65-46035 to IP and AO. This work was also supported by NIH/NCRR grant C06 RR018928 to Gladstone Institutes. We thank Dr. Kathryn Claiborn for editorial assistance.

Author contributions: AM, AI, IP, AO, MZ, and SSY carried out the study. MZ and YZ designed and coordinated the study, supervised the project, analyzed data, and wrote the manuscript. S.Y.Y.

managed mouse lines. Y.H. provided advice on study design and critically reviewed the manuscript.

Competing interests: Nothing to report.

Data and materials availability: All data associated with this study are available in the main text or the supplementary materials.